MULTIPLEX PURE ROTATIONAL COHERENT ANTI-STOKES RAMAN SPECTROSCOPY IN A MOLECULAR BEAM

Nicolaas Bloembergen, Kuei-Hsien Chen†, Cheng-Zai Lü, and Eric Mazur

Gordon McKay Laboratory, Harvard University, Cambridge, MA 02138

Pure rotational coherent anti-Stokes Raman spectroscopy using a single broadband dye-laser has been applied to study rotational energy distribution of molecules in a pulsed supersonic beam. The multiplex BOXCARS configuration allows accurate determination of rotational constants and rotational temperatures, and offers a great number of advantages over other methods. The technique was applied to calibrate the cooling effect of a pulsed molecular beam of N_2 and to study the rotational energy distributions of infrared multiphoton excited C_2H_4.

1. Introduction

Coherent anti-Stokes Raman spectroscopy (CARS) allows one to probe vibrational and rotational populations of gaseous and liquid samples with high spatial and temporal resolution [1]. For this reason CARS is widely used in spectroscopy and combustion diagnostics [1–3]. The predominant technique is *vibrational* CARS and involves a vibrational Raman transition [4]. Pure rotational CARS, which is associated with a rotational Raman transition, is particularly well suited for studying rotational energy distributions, and hence for low temperature measurements. In the pure rotational case, the linewidths are narrower and the Raman cross-sections larger than those for vibrational CARS and the signal intensity is larger.

The energy diagram of pure rotational CARS is shown in Fig. 1. Two lasers of frequency ω_1 and ω_2, with a frequency difference equal to the rotational Raman shift $\omega_R = \omega_1 - \omega_2$, coherently excite a transition between two rotational levels J and J', where J is the rotational quantum number. A third laser at frequency ω_3, which frequently is chosen equal to ω_1, scatters off this coherent excitation, and generates a CARS signal at a frequency $\omega_c = \omega_3 + \omega_R$. Since rotational Raman shifts are small (<20 cm^{-1}), the laser at

†Current address: General Electric CRD, P.O. Box 8, Schenectady, NY12301

J. Raman Spectroscopy 21, 819-825 (1990)

the Stokes frequency ω_2 must be tuned close to the laser at frequency ω_1, and a straightforward implementation of this scheme with a single dye-laser as in vibrational CARS is impractical. Therefore, pure rotational CARS is typically performed using an excimer laser or the second harmonic of a Nd:YAG laser to pump *two* closely-tuned dye lasers at frequencies ω_1 and ω_2 [5]. Alternatively, one can use the third-harmonic of a Nd:YAG laser to pump a Coumarin-based dye-laser at a frequency ω_2 close to the second-harmonic of the Nd:YAG laser at ω_1 ($\omega_2 = \omega_1 - \omega_R$) [6]. In both cases the setup is more cumbersome than the one for vibrational CARS.

The scheme can be significantly simplified, however, by deriving both ω_1 and ω_2 beams from one single broadband dye laser as shown in Fig. 2. Each rotational transition then selects pairs of photons at frequencies ω_1 and ω_2 within the bandwidth of the broadband beams, such that the frequency difference $\omega_1 - \omega_2$ matches the Raman shift ω_R. Since the rotational constants of molecules are small, a dye laser of 60 cm^{-1} bandwidth easily covers the entire rotational spectrum. Note that the frequency of the laser at ω_3 is not determined by any molecular parameters and may be chosen arbitrarily.

This broadband scheme, introduced by Eckbreth [7], has a number of advantages. First, since a photon at any frequency ω_1 within the bandwidth of the broadband laser automatically finds a corresponding photon at a frequency ω_2 such that $\omega_1 - \omega_2 = \omega_R$, *all* photons in the broadband beam are used. This contributes to a stronger CARS signal than in the vibrational scheme where only the resonant frequencies are used [7]. Second, since the center frequency of the broadband dye laser is arbitrary, one can choose the most efficient dye to improve the signal level. Third, the phase matching is the same for all molecules as long as the rotational Raman spectrum is covered by the broadband dye laser. Once the beams are properly aligned, therefore, one can switch from one molecule to another without any change in alignment.

To fulfill the phase matching condition, $k_C = k_1 - k_2 + k_3$, a number of possibilities exist: colinear, planar crossed-beam, and folded BOXCARS [1,8]. In this paper we demonstrate, for the first time, the use of multiplex [9] folded BOXCARS for pure rotational CARS with a single dye-laser. The three-dimensional phase-matching geometry is shown in Figs. 3a and 3b. Both k_1 and k_2 are derived from a single broadband dye laser, k_3 from a narrowband laser. Note that in this configuration the CARS beam is spatially separated from the pumping beam regardless of the magnitude of the rotational Raman shift. Also, the angle between k_1 and k_2 is much larger than that in the planar case. This avoids the use of a beam-combining dichroic mirror and the use of polarization to suppress the incident laser beams. Moreover one can easily switch back and forth between vibrational and pure rotational CARS by replacing one of the two broadband

beams by a second narrowband beam at ω_3. The same broadband laser can be used for both schemes because the center-frequency of the broadband laser is unimportant for the pure rotational scheme.

In pure rotational CARS spectra one can easily observe Stokes transitions in addition to the anti-Stokes transitions. These transitions, which are at the opposite end of the anti-Stokes transitions with respect to the position of the ω_3 laser beam, are referred to as coherent Stokes Raman spectroscopy lines (CSRS). The CSRS spectrum is a mirror image of the CARS spectrum.

2. Experimental

The experimental setup is shown in Fig. 4. The CARS laser beams are derived from the output of a Quantel YG471C Nd:YAG laser with a 10-ns pulse duration and a 200-mJ average second-harmonic output at 532 nm. An intracavity line-narrowing etalon reduces the linewidth to 0.05 cm^{-1}. About 50 mJ of the second harmonic is used for the ω_3 beam, while the remainder serves to pump a broadband dye laser-amplifier system generating the ω_1 and ω_2 beams. The prism-tuned broadband dye laser, operating on Fluorescein 548 dye around 550 nm, produces 2-mJ pulses of 6-ns pulse duration, and 60-cm^{-1} linewidth. These pulses are amplified to 30 mJ in two stages. All beams are vertically polarized, and are aligned parallel to one another before being focussed into the sample with a 25-cm focal length lens. The beam waist and the interaction length of the CARS beams are 80 μm and 200 μm, respectively.

The CARS beam generated in the interaction region passes through an aperture which spatially rejects the incident beams as shown in Fig. 4. The signal is then dispersed using a Jarrel Ash 78-420 1-m f/6.2 monochromator with a 0.05-Å resolution in second order. Instead of using the output slit of the monochromator, the dispersed CARS signal is recorded on the (horizontal) entrance slit of a Hamamatsu C1587 streak camera system with a 512 by 512 detector array. The resulting spectral resolution of the entire system is 0.12 Å. The dispersion of the monochromator was calibrated with the 6-Å separation of the two Na *D*-lines. For each spectrum an average over 50 laser shots is taken to obtain a good signal-to-noise ratio.

Experiments were done in bulk samples and in a supersonic molecular beam. In both cases the sample molecules can be excited by a third laser. In section 4 we report on the infrared-multiphoton-excitation [10,11,12] of ethylene with a CO_2-laser. For that purpose the molecules were irradiated with a 250-ns pulse from a grating-tuned TEA CO_2-laser

operating on the 9*P*14 line. The infrared beam is focused by a cylindrical lens in such a way as to overlap the focal region with the CARS interaction region. The time-evolution of the data can be obtained by triggering the streak-camera from the exciting laser pulse and using the time-resolution of the camera to obtain three-dimensional information of intensity versus wavelength and time [13].

The pulsed supersonic molecular beam apparatus consists of a nozzle mounted on a translational manipulator and a high vacuum chamber. The nozzle is a Toyota cold start fuel injector (model No. 23260-79055), which has been modified by machining off the fuel injection nozzle to a thickness of about 2 mm. The diameter D of the output aperture is 0.9 mm, and the pressure in the reservoir is between 1 and 3 atm. The nozzle is driven by a custom built electronic driver at a rate of 10 Hz with a variable opening time of 0.1 to 1 ms. The chamber is pumped by an Edwards E2M12 rotary pump and an Edwards MK2 700-liter/s diffusion pump. With the molecular beam off, the beam chamber pressure is 4×10^{-7} Torr; with a reservoir pressure of about 3 atm and 1-ms molecular pulses at a 10-Hz repetition rate, the chamber pressure rises to 7×10^{-4} Torr. The beam expands vertically downward into the high-vacuum chamber, which has four windows allowing laser excitation and CARS probing of the molecules in the beam. An *XYZ* translational manipulator allows one to overlap the molecular beam with the laser beams and to adjust the distance x between the nozzle and the interaction region.

3. Pure rotational CARS of N_2 in a molecular beam

The pure rotational CARS technique is ideally suited to measure the density and the rotational temperature profiles in the supersonic beam. The rotational CARS frequency shifts for a linear molecule ($\Delta J = 2$) are given by

$$\Delta\omega = B(J+2)(J+3) - BJ(J+1) = 6B + 4BJ, \quad (1)$$

where B is the rotational constant. The pure rotational CARS spectrum of nitrogen at room temperature is shown in Fig. 5. The peaks are separated by 8 cm^{-1} in excellent agreement with the rotational constant B for nitrogen. Note that for rotational Raman shifts much larger than the bandwidth of the broadband dye laser the signal falls off.

It is important to note here that the rotational CARS signal, like vibrational CARS, is determined by the resonant contribution of all rotational transitions to the third-order nonlinear susceptibility $\chi^{(3)}$, and is proportional to the square of the population difference between the initial and final rotational states involved in the Raman transition

[14]. For the intensity I_J corresponding to a rotational transition from initial state J, one obtains [8]

$$I_J \propto \left[\frac{d\sigma(J)}{d\Omega} \frac{N g_J (2J+1)}{Z_R} \left[e^{-J(J+1)B/kT} - e^{-(J+2)(J+3)B/kT} \right] \right]^2 \equiv \left[\frac{d\sigma(J)}{dW} \Delta N_J \right]^2 , \qquad (2)$$

where $d\sigma(J)/d\Omega$ is the Raman transition cross-section [15], N is the number density of the molecules, g_J the nuclear spin weight of the initial state, and Z_R the rotational partition function. Equation (2) can be used to evaluate the rotational temperature of the molecules from measured pure rotational spectra such as the one shown in Fig. 5.

The translational temperature of the sample is greatly reduced by the adiabatic expansion in the supersonic molecular beam. As the distance x from the nozzle increases, the isentropic temperature of molecules, T_i, decreases according to [16]:

$$T_i = \frac{T_o}{1 + \frac{1}{2}(g-1) M^2} , \qquad (3)$$

where T_o is the reservoir temperature, γ the specific heat ratio and M the Mach number, which can be obtained from an empirical relation [16]:

$$M = A \left(\frac{x - x_o}{D} \right)^{\gamma - 1} - \frac{1}{2} A^{-1} \frac{g+1}{g-1} \left(\frac{x - x_o}{D} \right)^{1-\gamma} . \qquad (4)$$

The constants A and x_o depend only on the specific heat ratio γ. Values for these constants can be found in the literature [17].

The adiabatic expansion not only cools the translational degrees of freedom, but indirectly, via collisions, also the vibrational and rotational degrees of freedom. Collisions near the nozzle equilibrate the vibrational and rotational temperatures with the translational one. As the gas expands, however, the collision rate decreases and the transfer of energy between the various degrees of freedom slows down. Generally, the translation-rotation relaxation rate is much higher than the translation-vibrational rate. Therefore the rotational temperature is usually lower than the vibrational one, and both are higher than the translational one [18].

Together with this decrease in temperature one has a decrease in sample pressure p [16]:

$$p = p_0 \left(\frac{T_i}{T_0} \right)^{1/(1-\gamma)}. \qquad (5)$$

As can be seen in Eq. (2), the CARS signal is proportional to the square of the number density N. Consequently the CARS signal will fall off rapidly when the distance x to the nozzle is increased.

The dramatic cooling of the rotational degree of freedom is evident from the spectra shown in Figs. 6 and 7. At a distance x/D = 5.2 from the nozzle (see Fig. 6) only states with $J \leq 4$ are populated. From a fit to a theoretical spectrum according to Eq. (2), one finds a rotational temperature of 30 K. This is identical to the isentropic temperature one obtains for N_2 from Eq. (3) at x/D = 5.2, indicating a very efficient rotational cooling. Still further away from the nozzle, at x/D = 11.6, the isentropic temperature according to Eq. (3) is 15 K. In the measured spectrum only states with $J \leq 2$ appear, see Fig. 7. The agreement between this spectrum and Eq. (2), however, is no longer very good. This is probably due to different cooling rates for the ortho and para modifications of N_2 [19].

The density in the supersonic jet can be determined by comparing the pure rotational CARS spectra from molecules in the beam with those obtained in the bulk. According to Eq. (2) the square root of the intensity of each peak in the spectrum corresponding to a certain J-value is proportional to the population difference ΔN_J between the J and J+2 states, so that:

$$\Delta N_J = c \left(\frac{d\sigma(J)}{dW} \right)^{-1} \sqrt{I_J} \ , \qquad (6)$$

where c is a proportionality constant which depends on the alignment. The total number density of the molecules is then given by

$$N = \sum N_J = \Delta N_0 + \Delta N_1 + 2\Delta N_2 + 2\Delta N_3 + 3\Delta N_4 + 3\Delta N_5 + \ldots . \qquad (7)$$

If one switches between bulk samples and molecular beam without change in alignment or detector gain the proportionality constant c remains unchanged. This allows one to determine the density by comparing the cN obtained from spectra taken in the beam with the one following from bulk measurements at a known pressure and temperature. For nitrogen at x/D = 4.5 one thus finds for the density in the jet 6×10^{23} m^{-3}.

Because of the high spatial resolution of the BOXCARS configuration one can map out the entire three-dimensional temperature and density profiles of the expanding beam using this technique. This allows one to completely characterize the flow and optimize

nozzle design. The results also clearly show that the technique yields excellent signal-to-noise even at very small (<5 cm^{-1}) Raman shift and extremely low densities.

4. Pure rotational CARS of infrared-multiphoton-excited ethylene

Ethylene is a nearly symmetric asymmetric top molecule. In general the rotational Raman spectra of asymmetric top molecules are difficult to analyze because of the many rotational degrees of freedom that cause large numbers of overlapping lines to appear in the spectrum. The selection rules for rotational Raman transitions of symmetric top molecules are [20]

$$\Delta J = 0, \pm 1, \pm 2, \Delta K = 0, \tag{8}$$

where J and K are the rotational quantum numbers corresponding to the angular momentum vector $\boldsymbol{J}$ and its projection on the figure axis of the molecule.

Ethylene has three rotational degrees of freedom. The rotation along the C=C axis has the largest rotational constant, but a small Raman cross section [20]. The other two rotational degrees of freedom have nearly identical rotational constants, making it difficult to resolve the spectrum by conventional Raman spectroscopy [21]. There are four branches in the rotational Raman spectrum as listed in Table 1 [21].

The pure rotational CARS spectrum of ethylene in the bulk at room temperature is shown in Fig. 8. The individual lines are clearly resolved and can be assigned to the four branches listed in Table 1. By blocking the strong laser background at zero Raman shift using a thin wire placed in front of the detector array, one can easily observe both CARS and CSRS spectra. Figure 9 shows such a spectrum for ethylene after expansion in the supersonic beam at x/D = 5.7. As can be seen, the rotational distribution of ethylene now peaks at much lower J-values. The spectrum becomes easier to assign because one can directly compare the Stokes and anti-Stokes lines instead of using the (estimated) position of the laser frequency to determine the Raman shifts. This allows one to determine the rotational constants for ethylene in a straightforward fashion.

The rotational constants obtained from the spectra in Figs. 8 and 9 are $\tilde{B} = \frac{1}{2}(B+C) = 0.92 \pm 0.01$ cm^{-1} and $C = 0.83 \pm 0.01$ cm^{-1}. For planar molecules the moments of inertia I about the three principal axes of rotation satisfy the relation

$$I_C = I_A + I_B\ , \tag{9}$$

where the subscript A labels the figure axis. The rotational constants are related to the moments of inertia by

$$A_i = \frac{h}{8p^2 I_{A_i}} \qquad (A_i = A,\ B,\ C)\ . \tag{10}$$

Equations (9) and (10) allow one to determine the three rotational constants from the values of $\tilde{B}$ and C. The resulting values listed in Table 2 are in excellent agreement with published values.

To study the effect of infrared excitation on the rotational spectrum, the ν_4-mode of the ethylene molecules was pumped with the 9*P*14 CO_2-laser line. The result is shown in Fig 10, where the dashed line is the rotational CARS spectrum of ethylene without infrared pumping and the solid one is the spectrum 250 ns after an infrared pulse of 6.3 J/cm^2. The lines corresponding to the $J = 1$ and $J = 2$ states are strongly reduced in intensity by the CO_2-laser, indicating a depletion of the corresponding rotational states.

If the CO_2-laser is tuned to a different line, one expects to observe a change in the rotational lines that are depleted. Indeed, when the laser is switched to the 9*P*10 line, it was found that the $J = 2$ and $J = 3$ states are considerably depleted. Detailed investigations of CO_2-laser excitation of several other molecules analyzed by CARS spectroscopy have been published elsewhere [13].

5. Conclusions

This paper presents a three-dimensional approach for phasematching in pure rotational multiplex CARS measurements with a single broadband dye laser. The technique has been applied to study the rotational cooling of N_2 in a supersonic beam, and the depletion of rotational levels in the infrared multiphoton excitation of C_2H_4.

For asymmetric top molecules — the majority of polyatomic molecules — the rotational spectra are complicated with many, frequently overlapping, branches. As shown by the data for C_2H_4, these spectra can still be resolved using the multiplex pure rotational CARS technique presented here. The technique therefore allows direct observation of laser-induced changes in rotational population. It should also be possible to study the rotational distributions of molecular fragments following laser-induced photodissociation.

Summarizing the results we conclude that:

1. The instrumentation is greatly simplified over previous approaches. In fact, it is identical to that for vibrational CARS and therefore it is relatively simple to switch back and forth between vibrational and pure rotational CARS. Since the scheme is independent of the frequency difference between the dye laser and its pump laser, not even a change of dye is required.
2. Since the rotational constants of molecules are all small, only one dye is required to measure different species. This means one can use this technique to monitor the rotational populations of a number of species simultaneously.
3. The method works extremely well even for Raman shifts as small as a few wavenumbers (see Figs. 8 through 10).
4. Because all photons within the broadband dye laser profile are used to generate a signal, the methods can be extended to even lower density than the vibrational CARS scheme.
5. The method permits a more detailed analysis of vibrational excitation by CO_2-laser pulses, both in the collisional and collisionless regimes.

Acknowledgments

We would like to acknowledge many useful discussions with Shrenik Deliwala and Jay Goldman. This work was supported by the Army Research Office contracts DAAL03-88-K-0114 and DAAL03-86-G-70098, the Joint Services Electronics Program contract N00014-84-K-0465, and by Hamamatsu Photonics K.K.

Figure captions:

Fig. 1 Energy diagram for pure rotational coherent anti-Stokes Raman spectroscopy (CARS).

Fig. 2 Schematic spectrum of broadband pure rotational CARS. The two pumping lasers at ω_1 and ω_2 are from a single broadband dye laser (broad solid curve). This laser provides pairs of photons with a frequency difference corresponding to the rotational Raman transition frequency ω_R. The ω_3 beam is a narrow band laser of arbitrary wavelength. The dashed curve indicates the accessible CARS frequencies that fall within the dye-laser profile.

Fig. 3 (a) Laser beam configuration for pure rotational CARS. (b) Phase matching diagram of pure rotational CARS.

Fig. 4 Experimental setup. SHG = second harmonic generation; L = lens; A = aperture; T = optional streak camera trigger for time-resolved studies.

Fig. 5 Pure rotational CARS spectrum of N_2 at room temperature. The label J labels the rotational quantum number of the initial Raman transition. Because the population of even and odd J states have a nuclear spin weight ratio of 2, the spectrum shows an alternating intensity distribution. The vertical scale is arbitrary.

Fig. 6 Pure rotational CARS spectrum of N_2 in a pulsed supersonic beam at x/D = 5.2. This spectrum corresponds to a rotational temperature of 30 K.

Fig. 7 Pure rotational CARS spectrum of N_2 in a pulsed supersonic beam at x/D = 11.6.

Fig. 8 Pure rotational CARS spectrum of ethylene in the bulk at room temperature and a pressure of 30 Torr. The assignment of *S, R,* S^* and R^* branches are described in Table 1.

Fig. 9 Pure rotational CARS and CSRS spectrum of ethylene in the beam at x/D = 5.7. The arrow indicates the position of the incident laser at ω_3. This wavelength has been physically blocked out in front of the detector array by a thin wire. Notice that all four *S, R,* S^*, R^* branches appear in each of the CARS and CSRS spectra.

For simplicity, only the S and R branches are assigned on the CSRS side, while the S^* and R^* branches are assigned on the CARS side.

Fig. 10 Pure rotational CARS spectra of ethylene in the beam at x/D = 5.7, without infrared excitation (dashed line) and 250 ns after 9P14 CO_2-laser excitation (solid line). Note the depletion of the J = 1 and J = 2 levels.

Tables:

Branch	Transition	Remarks
R	$\Delta J = 1$	Symmetric top part
S	$\Delta J = 2$	Symmetric top part
R^*	$\Delta J = 1$	Contribution of deviation from symmetric top
S^*	$\Delta J = 2$	Contribution of deviation from symmetric top

Table 1. Assignment of the four branches in the rotational Raman spectrum of ethylene.

	A (cm^{-1})	B (cm^{-1})	C (cm^{-1})
This work	4.66 ± 0.02	1.01 ± 0.01	0.83 ± 0.01
Ref. [22]	4.828	1.0012	0.8282
Ref. [21]	4.66 ± 0.20	1.008 ± 0.006	0.828 ± 0.003

Table 2. Comparison of the obtained C_2H_4 rotational constants with published values.

References

[1] J.W. Nibler and G.A. Pubanz, in *Advances in Non-linear spectroscopy* J.H. Clark and R.E. Hester, Eds. (John Wiley & Sons Ltd, 1988), pp. 78.

[2] R.P. Lucht, Opt. Lett. 12 (1987) 78.

[3] F.Y. Yueh and E.D. Beiting, Appl. Opt. 27 (1988) 3233.

[4] A.C. Eckbreth and T.J. Anderson, Appl. Opt. 23 (1984) 1328.

[5] B. Dick and A. Gierulski, Appl. Phys. B 40 (1986) 1.

[6] J.B. Zheng, J.B. Snow, D.V. Murphy, A. Leipertz, R.K. Chang and R.L. Farrow, Opt. Lett. 9 (1984) 341.

[7] A.C. Eckbreth and T.J. Anderson, Opt. Lett. 11 (1986) 496.

[8] J.A. Shirley, R.J. Hall and A.C. Eckbreth, Opt. Lett. 5 (1980) 380.

[9] W.B. Roh, P.W. Schreiber and J.P. Taran, Appl. Phys. Lett. 29 (1976) 174.

[10] W. Fuss and K.L. Kompa, Prog. Quant. Electr. 7 (1981) 117.

[11] N. Bloembergen and E. Yablonovitz, Physics Today 5 (1978) 23.

[12] D.S. King, in *Dynamics of the excited state* K.P. Lawley, Eds. (Wiley, New York, 1982), pp. 105.

[13] K.H. Chen, C.Z. Lü, L.A. Avilés, E. Mazur, N. Bloembergen and M.J. Shultz, J. Chem. Phys. 91 (1989) 1462.

[14] Y.R. Shen, *The principles of nonlinear optics* (Wiley & sons, New York, 1984).

[15] G. Placzek and E. Teller, Z. Physik 81 (1933) 209.

[16] J.B. Anderson, *Molecular Beam and Low Density Gas Dynamics* (Decker, New York, 1974).

[17] J.B. Anderson, AIAA Journal 10 (1972) 111.

[18] P. Huber-Walchli and J.W. Nibler, J.Chem.Phys. 76 (1982) 273.

[19] G. Luijks, S. Stolte and J. Reuss, Chem. Phys. 62 (1981) 217.

[20] G. Herzberg, *Infrared and Raman spectra of polyatomic molecules* (Van Nostrand,, New York, 1945).

[21] J. Romanko, T. Feldman, E.J. Stansbury and A. McKellar, Can. J. Phys. 32 (1954) 375.

[22] G. Herzberg, *Electronic Spectra of Polyatomic Molecules* (Van Nostrand, New York, 1966).

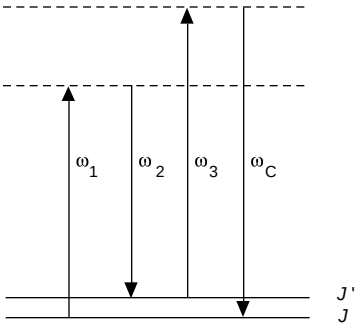

Fig. 1

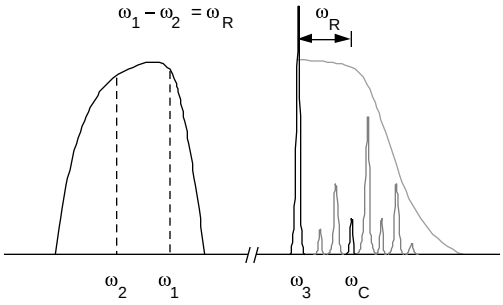

Fig. 2

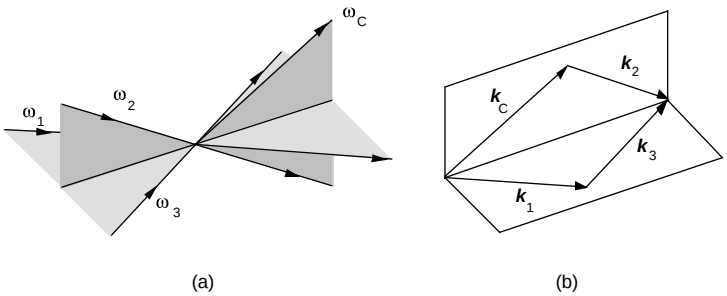

Fig. 3

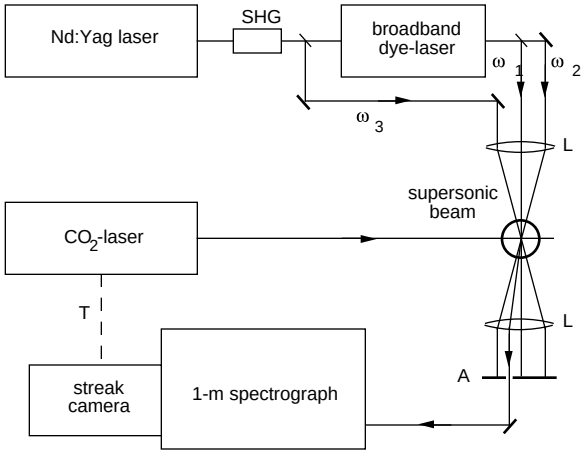

Fig. 4

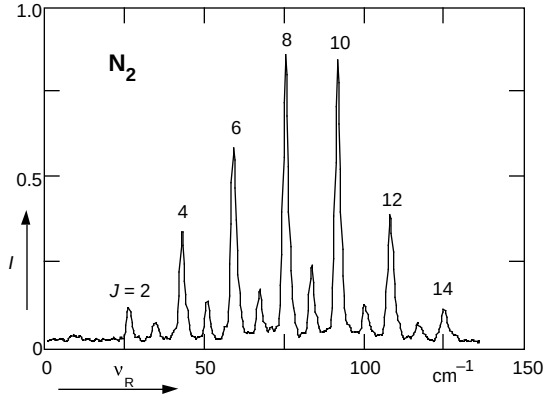

Fig. 5

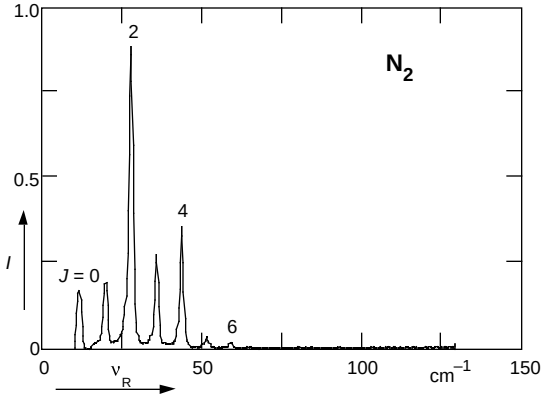

Fig. 6

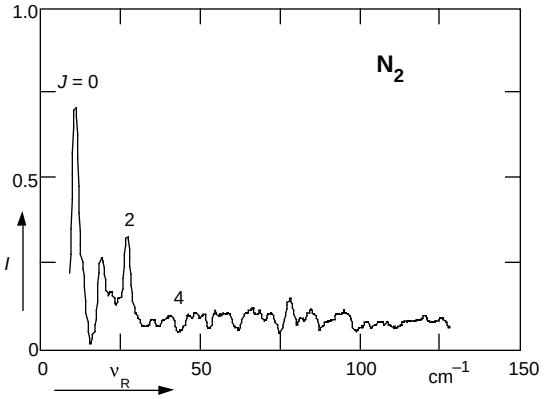

Fig. 7

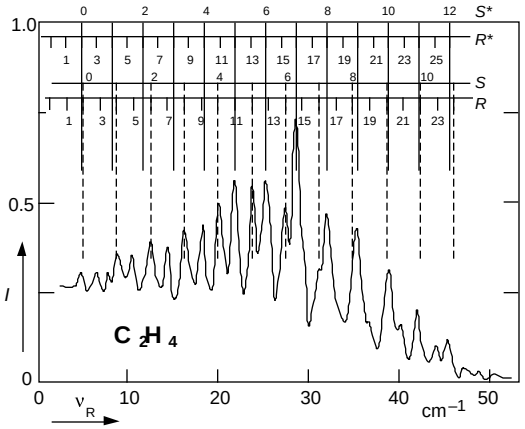

Fig. 8

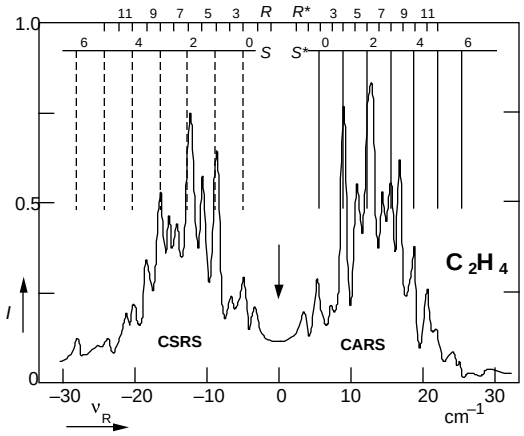

Fig. 9

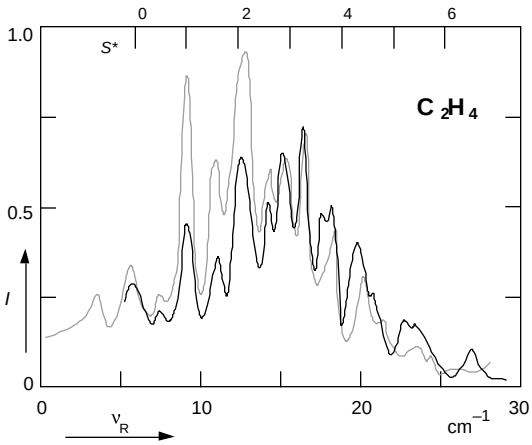

Fig. 10